Hiding in Plain View: Colloidal Self-Assembly from Polydisperse Populations

Bernard Cabane,[1,*] Joaquim Li,[2] Franck Artzner,[3] Robert Botet,[4] Christophe Labbez,[5] Guillaume Bareigts,[5]
Michael Sztucki,[6] and Lucas Goehring[2,†]
[1]*LCMD, CNRS UMR 8231, ESPCI, 10 rue Vauquelin, 75231 Paris Cedex 05, France*
[2]*Max Planck Institute for Dynamics and Self-Organization (MPIDS), 37077 Göttingen, Germany*
[3]*Institut de Physique de Rennes, CNRS UMR 6251, Université Rennes 1, 35042 Rennes Cedex, France*
[4]*Physique des Solides, CNRS UMR 8502, Université Paris–Sud, F-91405 Orsay, France*
[5]*ICB, CNRS UMR 6303, Université de Bourgogne Franche-Comté, F-21078 Dijon, France*
[6]*ESRF—The European Synchrotron, CS40220, 38043 Grenoble Cedex 9, France*

(Received 8 November 2015; revised manuscript received 10 March 2016; published 20 May 2016)

We report small-angle x-ray scattering experiments on aqueous dispersions of colloidal silica with a broad monomodal size distribution (polydispersity, 14%; size, 8 nm). Over a range of volume fractions, the silica particles segregate to build first one, then two distinct sets of colloidal crystals. These dispersions thus demonstrate fractional crystallization and multiple-phase (bcc, Laves AB_2, liquid) coexistence. Their remarkable ability to build complex crystal structures from a polydisperse population originates from the intermediate-range nature of interparticle forces, and it suggests routes for designing self-assembling colloidal crystals from the bottom up.

DOI: 10.1103/PhysRevLett.116.208001

What is the preferred structure for a population of colloidal particles, dispersed in liquid? This simple question has been satisfactorily answered only in the case of spherical particles that are effectively monodisperse in size [1–6]. As the volume fraction of particles increases, there is a well-defined transition from a liquid to a crystal state. Two types of structures can be found: close-packed and body-centered-cubic crystals; the preferred form depends on the range of the interparticle forces [5–7].

Polydisperse populations present a tougher problem. In one limit, for particles that interact as hard spheres, crystalline order is destroyed by even small amounts of polydispersity [3,4,8–10]. Charged particles interact instead via soft potentials and are more tolerant of polydispersity, especially where they have an *effectively* narrow size distribution, due to long-range interactions. In this other limit, a crystal state can be retained at low volume fractions, regardless of significant size polydispersity, if the interaction polydispersity remains low [6,11,12]. Between these two limits is a vast region of phase space where we do not know whether homogeneous crystallization or fractionated crystallization is possible.

Here, we address the self-organization of polydisperse populations of particles that interact through forces with an *intermediate* range, comparable to the variations in particle size. Using high-resolution scattering methods, we find that such populations can evolve through fractionated crystallization to yield coexisting crystals with different structures. These crystals can have large, complex unit cells with specific sites for particles of different sizes. To explain this result, we use numerical simulations to demonstrate how a broad distribution of particles can split spontaneously into different types of crystals, which cooperate to make the best use of the whole population.

The colloids that we have used are industrially produced. They consist of nanometric silica particles, dispersed in water (Ludox HS40). The particles are roughly spherical, with an average radius of 8 nm and a size polydispersity of 0.14 [13,14]. We used near-equilibrium dialysis to equilibrate them against NaCl solutions (5 mM, pH 9.5). They were then slowly concentrated by the addition of poly(ethylene glycol) to the solution outside the dialysis membranes, as in Refs. [14,15]. Under these conditions, the particles repel each other via a screened electrostatic interaction, with an effective Debye length of 2.5–4.5 nm, depending on their volume fraction ϕ. Further details of our methods and the dispersion properties (e.g., charge, equation of state, density) are given in the Supplemental Material [16].

Samples were characterized through small-angle x-ray scattering (SAXS), using ID02 at the ESRF. The strength of ordering in a colloidal dispersion can be evaluated by the height, $S_{\max}$, of the main peak of its effective structure factor $S(q)$, for scattering vector q [30–32]. $S(q)$ was found by dividing the radially averaged scattering intensity $I(q)$ by the form factor of a dilute ($\phi = 10^{-3}$) dispersion, and normalizing at high q, as in Refs. [14,32–34]. For low ϕ, these $S(q)$ had a broad main peak, indicative of disordered liquid arrangements of particles [Fig. 1(a)]. Indeed, all of these samples also behaved rheologically as fluids. The value of $S_{\max}$ (Table I) rose slowly with increasing ϕ, from 1.2 at $\phi = 0.04$, to 2.6 ± 0.1 at $\phi = 0.16$. Despite our polydispersity, which should lower $S_{\max}$ slightly [32,33] and add a low-q incoherent scattering [33,34], these values

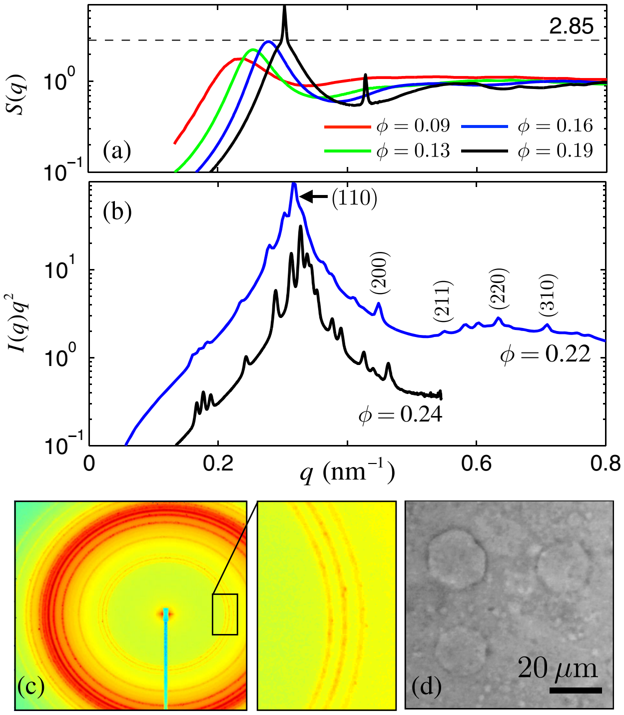

FIG. 1. (a) Effective structure factors. At low volume fractions, ϕ, the dispersion has a liquid structure, with broad peaks. When the intensity of the liquid peak would exceeded 2.85, bcc colloidal crystals appear alongside the liquid phase. (b) At higher ϕ, the scattering spectra show many sharp peaks in addition to the (indexed) bcc peaks. Their positions and relative intensities correspond to crystals of a Laves $MgZn_2$ phase, in coexistence with the bcc and liquid phases. (c) These diffraction patterns consist of spots arranged in rings and imply the existence of many micron-sized crystallites, which (d) can be seen directly by microscopy.

TABLE I. Sample summary, showing the volume fraction ϕ (± 0.005), the intensity of the liquid peak $S_{\max}$ and its predicted value (MSA) using Ref. [35], and the observed phases.

ϕ	$S_{\max}$ (liq.)	$S_{\max}$ (MSA)	Phases
0.038	1.2	1.33	liquid
0.046	1.4	1.40	liquid
0.057	1.5	1.50	liquid
0.067	1.6	1.58	liquid
0.079	2.2	1.69	liquid
0.085	1.8	1.74	liquid
0.128	2.2	2.12	liquid
0.131	2.1	2.15	liquid
0.159	2.7	2.42	liquid
0.161	2.5	2.44	liquid
0.188	⋯	2.72	liquid, bcc
0.207	⋯	2.94	liquid, bcc
0.219	⋯	3.08	liquid, bcc, Laves
0.235	⋯	3.28	liquid, bcc, Laves
0.240	⋯	3.35	liquid, bcc, Laves

agree well with the Hayter-Penfold mean spherical approximation (MSA) model [35] of monodisperse Yukawa spheres (Table I, using 8 nm particles with 5 mM salt and a surface charge of 170e).

At $\phi = 0.19$ and 0.21, we found that the 2D interference patterns of our dispersions also contained sharp diffraction spots, superimposed on the liquidlike scattering ring. The spots are the powder-diffraction pattern of small crystallites. Here, any fractionation between the liquid and crystals would invalidate the decomposition of $I(q)$ into a form factor and effective structure factor. Instead, we calculated the complex structure factor $F^2 \sim I(q)q^2$, which does not require knowledge of the form factors of each phase. The positions of the peaks of $F(q)$, as well as systematic extinctions ($h + k + l$ odd), indicated that they originated from colloidal crystals with a body-centered-cubic (bcc) structure [see Fig. 1]. This is in empirical agreement with liquid state theory, where, according to Verlet and Hansen [30,31], the liquid state with short-range order is unstable with respect to a crystalline structure when $S_{\max} > 2.85$. However, our dispersions were quite polydisperse, while the Verlet-Hansen criterion is strictly true only for monodisperse populations. Our observations suggest a possible reason why this agreement may still hold. It involves growing the bcc crystals from a narrow subset (i.e., an effectively monodisperse set) of the original population, and leaving the remaining particles in a liquid phase that coexists with these crystals.

As the dispersions were compressed to a higher ϕ, between 0.22 and 0.24, their scattering spectra became more complex. The interference patterns of these dispersions revealed a large number of spotty rings [Fig. 1(c)]. Typically, hundreds of spots were seen, whose diameters, $\delta \simeq 0.003$ nm^{-1}, imply the presence of many crystallites with a size of at least $\pi/\delta = 1$ μm. Microscope images [Fig. 1(d)] of such dispersions confirm the presence of stable, free-floating crystals.

In these spectra we detected, after radial averaging, a broad liquid peak, peaks from the bcc phase, and up to 14 additional well-resolved peaks, including a triplet at low q, implying the presence of a crystal phase with a large unit cell. The new peaks can all be indexed (see Table II and the Supplemental Material [16]) to the powder spectrum of a crystalline phase of compact hexagonal ($P6_3$/mmc) symmetry, with lattice constants $a = 43.58$ nm and $c = \sqrt{8/3}a$, and a unit-cell volume of $\sqrt{2}a^3 = 1.17 \times 10^5$ nm^3, in the $\phi = 0.235$ sample. In the same sample, the bcc peaks were indexed to a unit cell with lattice constant $a_{\mathrm{bcc}} = 27.11$ nm and volume $a_{\mathrm{bcc}}^3 = 1.99 \times 10^4$ nm^3. The unit-cell volume of the new phase is therefore 5.9 times larger than that of the coexisting bcc phase, which contains two particle sites per cell. Assuming that the number density of the sites is comparable in both phases—which, in conditions of close equilibrium and not too large fractionation, is reasonable—one finds that the new phase has 12 particles per unit cell.

TABLE II. Positions and relative scattering intensities of the observed and fitted diffraction peaks of the Laves phase, for $\phi = 0.235$. F is a complex structure factor corrected for the multiplicity of the peaks, m, and the averaging of the powder-diffraction pattern; zero indicates a systematic extinction, while not obs. indicates that a line was not observed experimentally.

h	k	l	m	q_{exp} (nm^{-1})	q_{fit} (nm^{-1})	F_{exp}	F_{fit}
0	0	1	2	not obs.	0.0883	not obs.	0
1	0	0	6	0.1667	0.1665	12.9	12.9
0	0	2	2	0.1769	0.1766	26.9	21.6
1	0	1	12	0.1885	0.1884	9.0	12.0
1	0	2	12	0.2431	0.2427	18.1	21.9
0	0	3	2	not obs.	0.2648	not obs.	0
1	1	0	6	0.2891	0.2883	84.3	84.3
1	1	1	12	not obs.	0.3015	not obs.	0
1	0	3	12	0.3132	0.3128	98.2	79.4
2	0	0	6	0.3329	0.3329	52.4	42.3
1	1	2	12	0.3378	0.3381	73.7	87.6
2	0	1	12	0.3441	0.3444	57.5	76.2
0	0	4	2	0.3530	0.3531	86.2	84.8
2	0	2	12	0.3767	0.3768	29.1	32.1
1	0	4	12	0.3903	0.3904	25.8	25.8
1	1	3	12	not obs.	0.3915	not obs.	0
2	0	3	12	0.4256	0.4254	19.6	18.2
2	1	0	12	0.4402	0.4404	8.4	10.0

One can reasonably expect that this phase is constituted by a mixture of nanoparticles with distinct mean diameters. Among the varied options [36], only one is of the compact hexagonal space group and contains 12 atoms per unit cell: the $MgZn_2$ Laves phase. Here, four Mg atoms sit on the four equivalent f Wyckoff positions, while eight Zn atoms are distributed on the six h and two a positions. This suggests that the new phase is composed of particles with two or three separate sizes organized into a Laves phase [37]. Within this hypothesis, the intensities of the Bragg peaks were fit with three free parameters corresponding to the radii r_a, r_f, and r_h of particles at the a, f, and h sites (see the Supplemental Material [16]). The fit, the results of which are shown in Table II, converges when $r_f = 9.1 \pm 0.3$ nm and $r_a = r_h = 7.3 \pm 0.3$ nm. The stoichiometry is consequently AB_2, with four large particles and eight small particles per unit cell. The larger particles occupy relatively spacious truncated tetrahedron environments, where they are comfortably surrounded by rings of smaller particles in octahedral sites (Fig. 2). In contrast to repulsive monodisperse crystals [2], the density of this Laves phase thus appears to be slightly lower (0.22) than that of the coexisting liquid (0.235); this situation could relate to the size selection of the individual sites.

Various AB_2 phases are well known in binary mixtures of hard spheres [38–43]. For example, the AlB_2 structure is a preferred crystal phase for binary mixtures with a size ratio of the smaller to larger particles between approximately 0.4 and 0.6 [39] and occurs in gem opals [40,41], while the $MgCu_2$ phase can be templated by walls [43]. What we have shown, however, is that similar phases also naturally arise in the solidification of broad and continuous populations of nanoparticles.

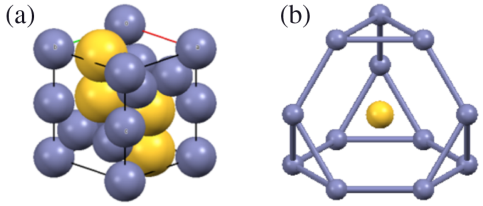

FIG. 2. (a) Unit cell of the Laves $MgZn_2$ phase. (b) Larger-than-average particles (yellow) occupy central sites and are surrounded by rings of smaller-than-average particles (blue).

An explanation for the coexistence of different crystal types, each composed of a subset of particle radii, can be made by seeking the equilibrium phases of the particle population. To this end, we investigated the fractionation of polydisperse charged particles through Gibbs-ensemble Monte Carlo numerical simulations [44] of a combination of a Laves $MgZn_2$ phase and a bcc phase, with a fcc phase added as a control. The model is similar to that used in Ref. [45]. Each phase was treated as an isolated volume (avoiding grain boundaries), but particles could move randomly between sites within each phase, and between phases, according to a Monte Carlo Metropolis algorithm at room temperature [46]. Although, for simplicity of demonstration, no colloidal liquid was modeled, we would expect such a phase to act as the medium of particle exchange and an acceptor of misfit particles. The proportions of particles and the lattice constants of the three phases were allowed to vary with volume exchange between them, keeping the total volume constant.

We considered a model of 22 466 particles with a Gaussian distribution of size r, an average radius of 8 nm, and a polydispersity of 0.14 [13], with a global $\phi = 0.22$. Interactions between particles were modeled as hard core plus Yukawa pair potentials, with an effective Debye length of $\kappa^{-1} = 2.8$ nm and an effective surface charge density of $0.2e/\mathrm{nm}^2$ (i.e., the charge on particle i scales as r_i^2). These parameters are estimated as in Ref. [25–27], accounting for modest charge renormalization, and they agree with the dispersion's experimentally determined equation of state [15,28].

Over time, the system evolved to find a configuration of minimal Madelung energy, and the proportion of each phase stabilized; Fig. 3 shows the final distribution of particle sizes, according to phases and sites. It shows how the coexistence of a Laves phase with the bcc phase is possible: the bcc phase uses the most populated part of the distribution of particle sizes, near the center of the distribution. In this example, a small minority of particles was also taken into the fcc phase, although this phase disappears if a longer screening length (3 nm) is used. In either case, the remaining particles have a bimodal size

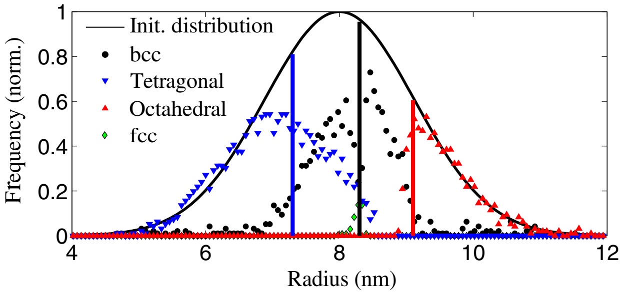

FIG. 3. Monte Carlo simulations of the fractionation of a polydisperse colloidal dispersion into three preset crystalline structures (bcc, fcc, Laves $\mathrm{MgZn_2}$). Shown are the final equilibrium particle-size distributions in each phase. The vertical lines show the average radii extracted from the SAXS data for particles in the bcc phase (black), and in the tetragonal (blue) and octahedral (red) sites of the Laves phase.

distribution and thus fit efficiently into the differently shaped sites of the Laves phase. Exploring various parameter values, we found that these results were robust to doubling the charge density of the particles, or letting their charge scale with r (as occurs for strong charge condensation [29]), but were sensitive to changes to the effective screening length (between 2.2 and 3.0 nm). The model's average radii of 7.0, 8.2, and 9.6 nm, for particles at equilibrium in the Laves tetragonal, bcc, and Laves octahedral sites, respectively, correspond well to the corresponding experimental values of 7.3, 8.3, and 9.1 nm.

We have thus described how a polydisperse population can split into coexisting phases of a colloidal liquid, a bcc crystal that preferentially selects the most abundant particle sizes, and a Laves phase that accommodates the remaining binary distribution of particles. This segregation by particle size is known as fractionated crystallization; similar processes are known in molecular systems [47], including geochemistry [48]. For hard-sphere colloids fractionation has been predicted beyond a terminal polydispersity of about 6% [49–53]. For medium-range Yukawa interactions (where κa is between 2.5 and 10), recent simulations [54] have suggested that a size polydispersity of 10%–15%, comparable to ours, is required to hinder crystallization, and thus to potentially trigger fractionation.

Experimentally, the best prior evidence of colloidal fractionation is the work of van Megen and collaborators [10,55,56], who invoke it to explain the nucleation processes of colloidal crystals near a terminal polydispersity. The coexistence of multiple solid phases is also known in cases of low-dimensional systems such as platelets [57] or particles confined to a plane [58]. Further evidence may also be hiding in old data such as Fig. 13 of Ref. [59], which appears to imply the presence of large-unit-cell crystals in dispersions similar to ours (10.2 nm silica with 9% size polydispersity).

The fractionation of particles in our experiments depends on their intermediate range of interactions. Much work on colloidal crystals is performed with particles that interact as hard spheres, and which crystallize when they are in close to direct contact, at $\phi \sim 0.5$. When such particles have a broad distribution of sizes, the unavoidable overlaps of any large adjacent particles inhibit the formation of a structure with long-range order [3,4,8,53], and dynamic arrest turns the dispersion into a glass [2,8]. Our particles interact instead through soft potentials. Assuming an effective Yukawa potential [25–27], the pair potential of two average-sized particles reaches about 3 kT at a volume fraction of 20%, corresponding to a surface separation (for bcc) of 8 nm. In this state, overlap of the particles themselves is still a rare occurrence, determined by the frequency of very large particles. These few "outliers" can easily be rejected away from the surfaces of growing crystals, as the soft potentials also keep the mobility of such particles high.

The width of the particle-size distribution and the range of particle interactions together control the frequency of such outliers, which are then available to build more diverse structures. We consider three cases. If the interactions are long range (with an effective diameter $\gg a$), then variations in the particle size will be screened, and simple fcc or bcc crystals are both expected and seen [1,6,11,12]. If the interaction range is intermediate—for example, $\kappa a \sim 1$—but the polydispersity σ is too high, then there will be too many overlaps to nucleate the first bcc crystals, and the dispersion may remain in a liquid or glass phase. Inverting Pusey's criterion [8] suggests that this will be the case when $\phi \geq c(1/(1+\sigma))^3$, where the order-1 constant c depends on how tolerant a crystal is to overlaps. If, however, the effects of the soft potential and the number of overlaps are balanced against each other, as in this Letter, then fractionation is encouraged, and the phase space of polydisperse colloidal dispersions is opened.

The behavior of such polydisperse nanometric dispersions points to directions that have not been explored thus far, despite theoretical predictions [49,51–54,60]. We demonstrate here fractionated crystallization, with the coexistence of at least three very different phases (liquid, bcc, and Laves), and the formation of complex crystals that efficiently utilize the full size distribution. The link between the particle-size distribution and the structures also gives us a scheme for generating even more complex phases through the crystallization of populations of particles with broader size distributions, provided that they interact through soft medium-range potentials. The variety of structures waiting to be discovered could be enormous, given that, within the limits defined above, there exists a huge phase space of different size distributions and interaction potentials to explore.

---

[*] bernard.cabane@espci.fr
[†] lucas.goehring@ds.mpg.de

[1] A. Kose, M. Ozaki, K. Takano, Y. Kobayashi, and S. Hachisu, J. Colloid Interface Sci. **44**, 330 (1973).

[2] P. N. Pusey and W. van Megen, Nature (London) **320**, 340 (1986).

[3] P. N. Pusey, E. Zaccarelli, C. Valeriani, E. Sanz, W. C. K. Poon, and M. E. Cates, Phil. Trans. R. Soc. A **367**, 4993 (2009).

[4] W. C. K. Poon, in *The Oxford Handbook of Soft Condensed Matter*, edited by E. M. Terentjev and D. A. Weitz (Oxford University Press, New York, 2015), Chap. 1.

[5] Y. Monovoukas and A. P. Gast, J. Colloid Interface Sci. **128**, 533 (1989).

[6] W. B. Russel, D. A. Saville, and W. R. Schowalter, *Colloidal Dispersions* (Cambridge University Press, Cambridge, England, 1989), p. 525.

[7] A. Yethiraj and A. van Blaaderen, Nature (London) **421**, 513 (2003).

[8] P. N. Pusey, J. Phys. (Paris) **48**, 709 (1987).

[9] S. R. Williams, I. K. Snook, and W. van Megen, Phys. Rev. E **64**, 021506 (2001).

[10] H. J. Schöpe, G. Bryant, and W. van Megen, Phys. Rev. E **74**, 060401 (2006).

[11] M. E. Leunissen, A. van Blaaderen, A. D. Hollingsworth, M. T. Sullivan, and P. M. Chaikin, Proc. Natl. Acad. Sci. U.S.A. **104**, 2585 (2007).

[12] N. J. Lorenz, H. J. Schöpe, H. Reiber, T. Palberg, P. Wette, I. Klassen, D. Holland-Moritz, D. Herlach, and T. Okubo, J. Phys. Condens. Matter **21**, 464116 (2009).

[13] V. Goertz, N. Dingenouts, and H. Nirschl, Part. Part. Syst. Charact. **26**, 17 (2009).

[14] J. Li, B. Cabane, M. Sztucki, J. Gummel, and L. Goehring, Langmuir **28**, 200 (2012).

[15] B. Jönsson, J. Persello, J. Li, and B. Cabane, Langmuir **27**, 6606 (2011).

[16] See Supplemental Material at http://link.aps.org/supplemental/10.1103/PhysRevLett.116.208001, which includes Refs. [13–15,17–29], for an extended materials and methods section, and for details of the powder spectra analyses.

[17] K. Wong, B. Cabane, and R. Duplessix, J. Colloid Interface Sci. **123**, 466 (1988).

[18] *Colloidal Silica: Fundamentals and Applications*, edited by H. E. Bergna and W. O. Roberts (Taylor & Francis, London, 2005), p. 895.

[19] *The Chemistry of Silica: Solubility, Polymerization, Colloid and Surface Properties and Biochemistry of Silica*, edited by R. K. Iler (Wiley, New York, 1979), p. 896.

[20] A. van Blaaderen and A. Vrij, J. Colloid Interface Sci. **156**, 1 (1993).

[21] V. M. Masalov, N. S. Sukhinina, E. A. Kudrenko, and G. A. Emelchenko, Nanotechnology **22**, 275718 (2011).

[22] F. Boulogne, L. Pauchard, F. Giorgiutti-Dauphiné, R. Botet, R. Schweins, M. Sztucki, J. Li, B. Cabane, and L. Goehring, Europhys. Lett. **105**, 38005 (2014).

[23] G. H. Bolt, J. Phys. Chem. **61**, 1166 (1957).

[24] J. Persello, in *Adsorption on Silica Surfaces*, edited by E. Papirer (Marcel Dekker, New York, 2000), Chap. 10.

[25] S. Alexander, P. M. Chaikin, P. Grant, G. J. Morales, P. Pincus, and D. Hone, J. Chem. Phys. **80**, 5776 (1984).

[26] L. Belloni, Colloids Surf. A **140**, 227 (1998).

[27] E. Trizac, L. Bocquet, M. Aubouy, and H. H. von Grünberg, Langmuir **19**, 4027 (2003).

[28] J. Li, M. Turesson, C. A. Haglund, B. Cabane, and M. Skepö, Polymer **80**, 205 (2015).

[29] N. Garbow, M. Evers, T. Palberg, and T. Okubo, J. Phys. Condens. Matter **16**, 3835 (2004).

[30] L. Verlet, Phys. Rev. **165**, 201 (1968).

[31] J.-P. Hansen and L. Verlet, Phys. Rev. **184**, 151 (1969).

[32] P. van Beurten and A. Vrij, J. Chem. Phys. **74**, 2744 (1981).

[33] B. D'Aguanno and R. Klein, J. Chem. Soc., Faraday Trans. **87**, 379 (1991).

[34] J. S. Pedersen, J. Appl. Crystallogr. **27**, 595 (1994).

[35] J. B. Hayter and J. Penfold, Mol. Phys. **42**, 109 (1981).

[36] L. Filion and M. Dijkstra, Phys. Rev. E **79**, 046714 (2009).

[37] R. L. Berry and G. B. Raynor, Acta Crystallogr. **6**, 178 (1953).

[38] P. Bartlett, R. H. Ottewill, and P. N. Pusey, Phys. Rev. Lett. **68**, 3801 (1992).

[39] A. B. Schofield, P. N. Pusey, and P. Radcliffe, Phys. Rev. E **72**, 031407 (2005).

[40] J. V. Sanders, Philos. Mag. A **42**, 705 (1980).

[41] M. J. Murray and J. V. Sanders, Philos. Mag. A **42**, 721 (1980).

[42] E. V. Shevchenko, D. V. Talapin, C. B. Murray, and S. O'Brien, J. Am. Chem. Soc. **128**, 3620 (2006).

[43] A.-P. Hynninen, J. H. J. Thijssen, E. C. M. Vermolen, M. Dijkstra, and A. van Blaaderen, Nat. Mater. **6**, 202 (2007).

[44] A. Z. Panagiotopoulos, N. Quirke, M. Stapleton, and D. J. Tidesley, Mol. Phys. **63**, 527 (1988).

[45] R. Botet, B. Cabane, L. Goehring, J. Li, and F. Artzner, Faraday Discuss. **186**, 229 (2016).

[46] D. Landau and K. Binder, *A Guide to Monte Carlo Simulation in Statistical Physics* (Cambridge University Press, Cambridge, England, 2000).

[47] R. E. Timms, Eur. J. Lipid Sci. Technol. **107**, 48 (2005).

[48] M. S. Ghiorso, Contrib. Mineral. Petrol. **90**, 107 (1985).

[49] P. Bartlett, J. Chem. Phys. **109**, 10970 (1998).

[50] P. Bartlett, Prog. Colloid Polym. Sci. **115**, 137 (2000).

[51] M. Fasolo and P. Sollich, Phys. Rev. Lett. **91**, 068301 (2003).

[52] P. Sollich and N. B. Wilding, Phys. Rev. Lett. **104**, 118302 (2010).

[53] P. G. Bolhuis and D. A. Kofke, Phys. Rev. E **54**, 634 (1996).

[54] M. N. van der Linden, A. van Blaaderen, and M. Dijkstra, J. Chem. Phys. **138**, 114903 (2013).

[55] S. Martin, G. Bryant, and W. van Megen, Phys. Rev. E **67**, 061405 (2003).

[56] H. J. Schöpe, G. Bryant, and W. van Megen, Phys. Rev. Lett. **96**, 175701 (2006).

[57] D. V. Byelov, M. C. D. Mourad, I. Snigireva, A. Snigirev, A. V. Petukhov, and H. N. W. Lekkerkerker, Langmuir **26**, 6898 (2010).

[58] N. Geerts, S. Jahn, and E. Eiser, J. Phys. Condens. Matter **22**, 104111 (2010).

[59] J. Chang, P. Lesieur, M. Delsanti, L. Belloni, C. Bonnet-Gonnet, and B. Cabane, J. Phys. Chem. **99**, 15993 (1995).

[60] L. A. Fernández, V. Martin-Mayor, and P. Verrocchio, Phys. Rev. Lett. **98**, 085702 (2007).